







ARTICLE

Coinfection with influenza A virus enhances SARS-CoV-2 infectivity

Lei Bai¹, Yongliang Zhao¹, Jiazhen Dong¹, Simeng Liang¹, Ming Guo¹, Xinjin Liu¹, Xin Wang¹, Zhixiang Huang¹, Xiaoyi Sun¹, Zhen Zhang¹, Lianghui Dong¹, Qianyun Liu¹, Yucheng Zheng¹, Danping Niu¹, Min Xiang¹, Kun Song¹, Jiajie Ye¹, Wenchao Zheng¹, Zhidong Tang¹, Mingliang Tang¹, Yu Zhou¹ , Chao Shen¹, Ming Dai², Li Zhou^{1,2} , Yu Chen¹ , Huan Yan¹, Ke Lan^{1,2,3}  and Ke Xu¹

The upcoming flu season in the Northern Hemisphere merging with the current COVID-19 pandemic raises a potentially severe threat to public health. Through experimental coinfection with influenza A virus (IAV) and either pseudotyped or live SARS-CoV-2 virus, we found that IAV preinfection significantly promoted the infectivity of SARS-CoV-2 in a broad range of cell types. Remarkably, in vivo, increased SARS-CoV-2 viral load and more severe lung damage were observed in mice coinfecting with IAV. Moreover, such enhancement of SARS-CoV-2 infectivity was not observed with several other respiratory viruses, likely due to a unique feature of IAV to elevate ACE2 expression. This study illustrates that IAV has a unique ability to aggravate SARS-CoV-2 infection, and thus, prevention of IAV infection is of great significance during the COVID-19 pandemic.

Cell Research (2021) 31:395–403; <https://doi.org/10.1038/s41422-021-00473-1>

INTRODUCTION

The outbreak of severe acute respiratory syndrome coronavirus 2 (SARS-CoV-2) at the end of 2019 has led to a worldwide pandemic. Until 13 January 2021, there have been more than 90 million confirmed infection cases and 1.9 million deaths globally (<https://covid19.who.int/>). The ending time and the final severity of the current COVID-19 pandemic wave are still uncertain. Meanwhile, the influenza season is merging with the current pandemic, potentially bringing more challenges and posing a larger threat to public health. There are many debates on whether seasonal flu will impact the severity of the COVID-19 pandemic and whether influenza vaccination is necessary for the coming winter. However, no experimental evidence is available concerning IAV and SARS-CoV-2 coinfection.

It is well known that the disease symptoms of SARS-CoV-2 and IAV infection symptoms are quite similar, including fever, cough, pneumonia, and acute respiratory distress syndrome.^{1,2} Moreover, both SARS-CoV-2 and IAV are airborne transmitted pathogens that infect the same human tissues, namely, the respiratory tract and nasal, bronchial, and alveolar epithelial cultures.^{3,4} In addition, alveolar type II cells (AT2 pneumocytes) appear to be preferentially infected by SARS-CoV-2 and are also the primary site of IAV replication.^{5,6} Therefore, overlap of the COVID-19 pandemic and seasonal influenza might place a large population under high risk for concurrent infection with these two viruses.⁷

Unfortunately, during the last winter flu season in the southern hemisphere, little epidemiological evidence was collected regarding the interaction between COVID-19 and flu, likely due to a low IAV infection rate resulting from social distancing.⁸ One case report showed that three out of four SARS-CoV-2 and IAV coinfecting patients rapidly develop respiratory deterioration.⁹ In

contrast, another study only reported mild symptoms in limited coinfection outpatients.¹⁰ A retrospective study found that the coinfection rate of SARS-CoV-2 and influenza virus was as high as 57.3% (among which 49.8% was coinfecting with IAV) in a single-centered study of 307 COVID-19 patients during the outbreak period in Wuhan.¹¹ Thus, the high coinfection rate and the unpredictable clinical outcomes pose great concerns when facing the threat of both viruses.

In this study, we tested whether IAV infection could affect the subsequent SARS-CoV-2 infection in both cultured cells and mice. Our results demonstrate that preinfection with IAV strongly enhances the infectivity of SARS-CoV-2 by boosting viral entry into cells and elevating the viral load, leading to more severe lung damage in infected mice. These data suggest a clear auxo-action of IAV on SARS-CoV-2 infection, which underscores the great risk of influenza virus and SARS-CoV-2 coinfection to public health.

RESULTS

IAV promotes SARS-CoV-2 virus infectivity

To study the interaction between IAV and SARS-CoV-2, A549 (a hypotriploid alveolar basal epithelial cell line) cells that are susceptible to IAV infection but usually do not support SARS-CoV-2 infection were applied to test whether IAV preinfection would modulate the infectivity of SARS-CoV-2. Pseudotyped VSV luciferase-reporter particles bearing SARS-CoV-2 spike protein (pseudo-SARS-CoV-2) were used to visualize the viral entry.¹² The cells were first infected with IAV (A/WSN/1933(H1N1)) or mock-infected for 6 h, 12 h, or 24 h and then infected with the pseudo-SARS-CoV-2 virus for another 24 h (experimental scheme shown in Fig. 1a). The data in Fig. 1b show that A549 cells became highly

¹State Key Laboratory of Virology, College of Life Sciences, Wuhan University, Wuhan, Hubei 430072, China; ²Animal Biosafety Level 3 Laboratory, Wuhan University, Wuhan, Hubei 430072, China and ³Frontier Science Center for Immunology and Metabolism, Wuhan University, Wuhan, Hubei 430072, China

Correspondence: Ke Lan (kulan@whu.edu.cn) or Ke Xu (xuke03@whu.edu.cn)

These authors contributed equally: Lei Bai, Yongliang Zhao, Jiazhen Dong, Simeng Liang, Ming Guo.

Received: 1 November 2020 Accepted: 18 January 2021

Published online: 18 February 2021

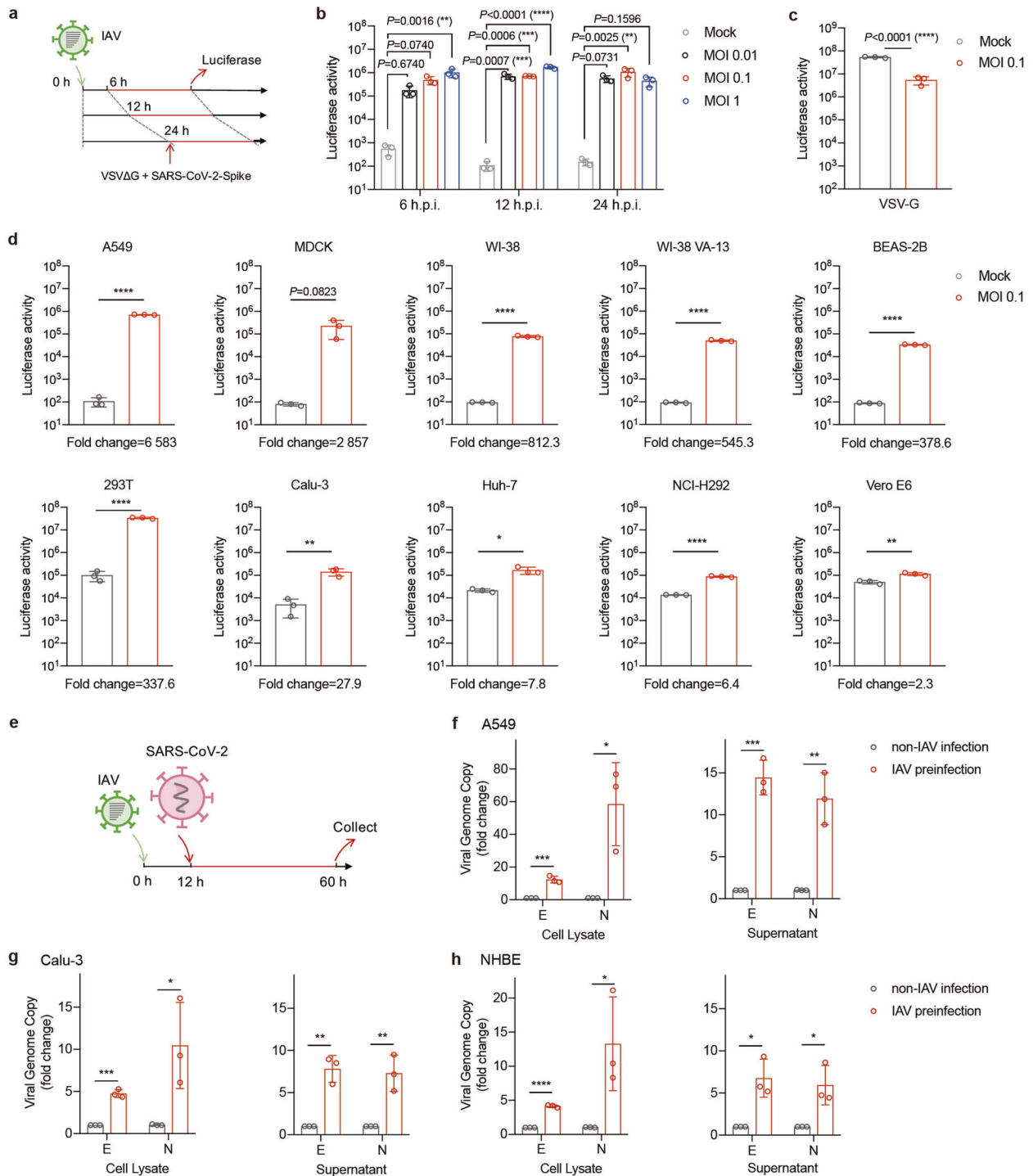


Fig. 1 IAV promotes SARS-CoV-2 virus infectivity. **a** Diagram of the experimental procedure. **b** A549 cells were infected with A/WSN/33 (WSN) at the indicated MOIs. At 6, 12, and 24 h post-IAV infection, cells were infected with pseudo-SARS-CoV-2 for another 24 h. Luciferase activity was measured to reflect virus entry efficiency. *P* values are from unpaired one-way ANOVA. **c** A549 cells were infected with WSN at an MOI of 0.1. At 12 h post-IAV infection, cells were infected with VSV-G-Luc for another 24 h. Luciferase activity was measured to reflect virus entry efficiency. **d** The indicated cells were infected with WSN at an MOI of 0.1. At 12 h post-IAV infection, cells were infected with pseudo-SARS-CoV-2 for another 24 h. Luciferase activity was measured to reflect virus entry efficiency. **e** Experimental procedure of IAV and live SARS-CoV-2 coinfection. A549 (f), Calu-3 (g), and NHBE (h) cells were preinfected with WSN at an MOI of 0.1 for 12 h. Cells were then infected with live SARS-CoV-2 at an MOI of 0.01 for another 48 h. Total RNA in cell lysates and the supernatants was collected to detect the E and N genes via TaqMan-qRT-PCR. The data are expressed as fold changes in viral RNA levels in IAV preinfected cells relative to the non-IAV infection control. Values represent means ± SD of three independent experiments. **P* < 0.05, ***P* < 0.01, ****P* < 0.001, *****P* < 0.0001.

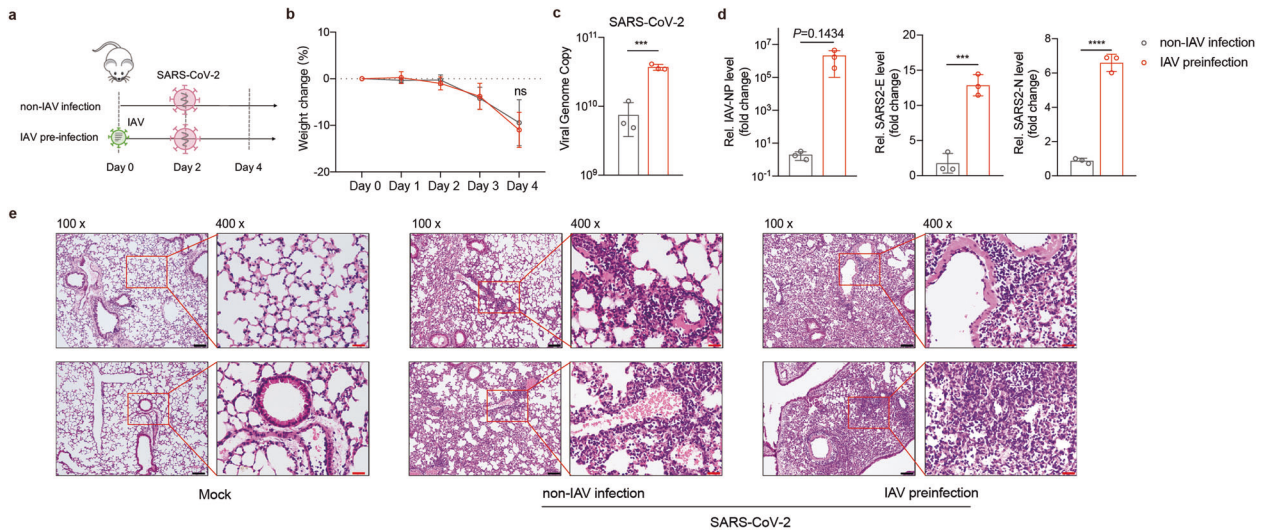


Fig. 2 IAV and SARS-CoV-2 coinfection induced more severe pathology in infected mice. **a** Diagram of the experimental procedure. K18-hACE2 transgenic mice were first intranasally infected with 2000 PFU of WSN or PBS on day 0. Two days post-IAV infection, mice were intranasally infected with 3×10^5 live SARS-CoV-2 or PBS. On day 4, half of the lung tissues collected from all the mice were homogenized to detect RNA or protein levels. **b** The body weights and survival were monitored until day 4 (non-IAV treatment group, $n = 4$; IAV preinfection group, $n = 4$). The dotted lines indicate the initial weight. The body weights are presented as the mean percentage of weight change \pm SD. **c** The viral genome copy numbers of SARS-CoV-2 N were quantified. Values represent means \pm SD of three individual mice. **d** The relative mRNA levels of IAV NP (**d, left**), SARS-CoV-2 E (**d, middle**) and the N gene (**d, right**) were measured from lung homogenates in the indicated groups and normalized to GAPDH for the individual mouse. The data are expressed as fold changes relative to the non-IAV infection control. Values represent means \pm SD of three individual mice. **e** Histopathologic and immunohistochemical studies were performed with lung slide samples in the indicated groups **c–d**. * $P < 0.05$, ** $P < 0.01$, *** $P < 0.001$, **** $P < 0.0001$.

sensitive (up to 10,000-fold) to the pseudo-SARS-CoV-2 virus after infection with IAV at different doses (from a low MOI of 0.01 to a high MOI of 1, also shown by pseudo-SARS-CoV-2 with an mCherry reporter in Supplementary information, Fig. S1a). In contrast, preinfection with IAV had no impact on pseudotyped VSV particles bearing VSV-G protein (Fig. 1c). We further tested more cell lines and showed that the enhancement of pseudo-SARS-CoV-2 infectivity by IAV was a general effect, although with different degrees (Fig. 1d).

To validate the above results, we substituted pseudo-SARS-CoV-2 with live SARS-CoV-2 (experimental scheme shown in Fig. 1e). We found that preinfection with IAV strongly increased the copy number of the SARS-CoV-2 genome (E (envelop) and N (nucleocapsid) genes) in both A549 cell lysates (~12- to 58-fold) and supernatants (~10- to 15-fold) (Fig. 1f). Notably, in Calu-3 (Fig. 1g) and NHBE (Fig. 1h) cells that are inherently susceptible to SARS-CoV-2, IAV preinfection further increased SARS-CoV-2 infectivity by > 5 -fold.

Collectively, these data suggest an auxo-action of IAV on SARS-CoV-2 in a broad range of cell types.

IAV and SARS-CoV-2 coinfection in mice results in increased SARS-CoV-2 viral load and more severe lung damage

The K18-hACE2 transgenic mice were used to study the interaction between IAV and SARS-CoV-2 in vivo. Mice were infected with 3×10^5 PFU of SARS-CoV-2 with or without preinfection with 2000 PFU of IAV and were then sacrificed two days after SARS-CoV-2 infection (the experimental scheme is shown in Fig. 2a). The data in Fig. 2b show that there were no significant differences in the body weights of mice between groups within 4 days post-infection (d.p.i.). The viral RNA genome copies from lung homogenates confirmed that SARS-CoV-2 efficiently infected both groups (more than 4×10^9 N gene copies) (Fig. 2c). By contrast, the influenza NP gene was only detected in the IAV preinfection group (Fig. 2d left). Intriguingly, a significant increase in SARS-CoV-2 viral load was observed in lung homogenates from coinfecting mice compared to homogenates

from SARS-CoV-2 single-infected mice (Fig. 2d middle, 12.9-fold increase in E gene; Fig. 2d right, 6.6-fold increase in N gene). Moreover, there were no significant differences in SARS-CoV-2 viral loads from brains between the single-infected and coinfecting mice indicating that coinfection mainly occurred in the lung of infected animals (Supplementary information, Fig. S2). The lung histological data in Fig. 2e further illustrate that IAV and SARS-CoV-2 coinfection induced more severe lung pathologic changes, with massive cell infiltration and obvious alveolar necrosis, compared to SARS-CoV-2 single infection or mock infection.

IAV specifically facilitates SARS-CoV-2 infection

We further tested whether several other respiratory-transmitted viruses had similar promotive effects on SARS-CoV-2 infection. For this, A549 cells were infected with SARS-CoV-2 with or without human respiratory syncytial virus (HRSV), human parainfluenza virus (HPIV), or human rhinovirus 3 (HRV3), respectively. To our surprise, none of HRSV (Fig. 3a), HPIV (Fig. 3b), or HRV3 (Fig. 3c) could stimulate pseudo-SARS-CoV-2 infection at neither low nor high infection dose. Quantification of viral genes from HRSV, HPIV, and HRV3 guaranteed the efficient infection of these viruses at 12 h post-infection (h.p.i.) (Fig. 3d–f). Live SARS-CoV-2 virus results also showed no induction under the preinfection of HRSV (Fig. 3g), (Fig. 3h), or HRV3 (Fig. 3i). Again, viral genes from HRSV, HPIV, and HRV3 were quantified at 60 h.p.i. to confirm the sufficient infection of these viruses (Fig. 3j–l). Taken together, these data suggest that IAV has a unique feature to promote both pseudo- and live-SARS-CoV-2 infection compared to HRSV, HPIV, and HRV3.

IAV infection induces elevated ACE2 expression

As IAV strongly increased pseudo-SARS-CoV-2 infection, we examined the viral entry process. It has been reported that the cellular receptor angiotensin-converting enzyme 2 (ACE2),^{13–15} together with transmembrane serine protease 2 (TMPRSS2),¹⁶ Furin¹⁷ and cathepsin L (CatL),^{18,19} mediates SARS-CoV-2 viral entry. In IAV-infected cells, we found that the mRNA levels of ACE2 and TMPRSS2, but not those of Furin and CatL, were increased by

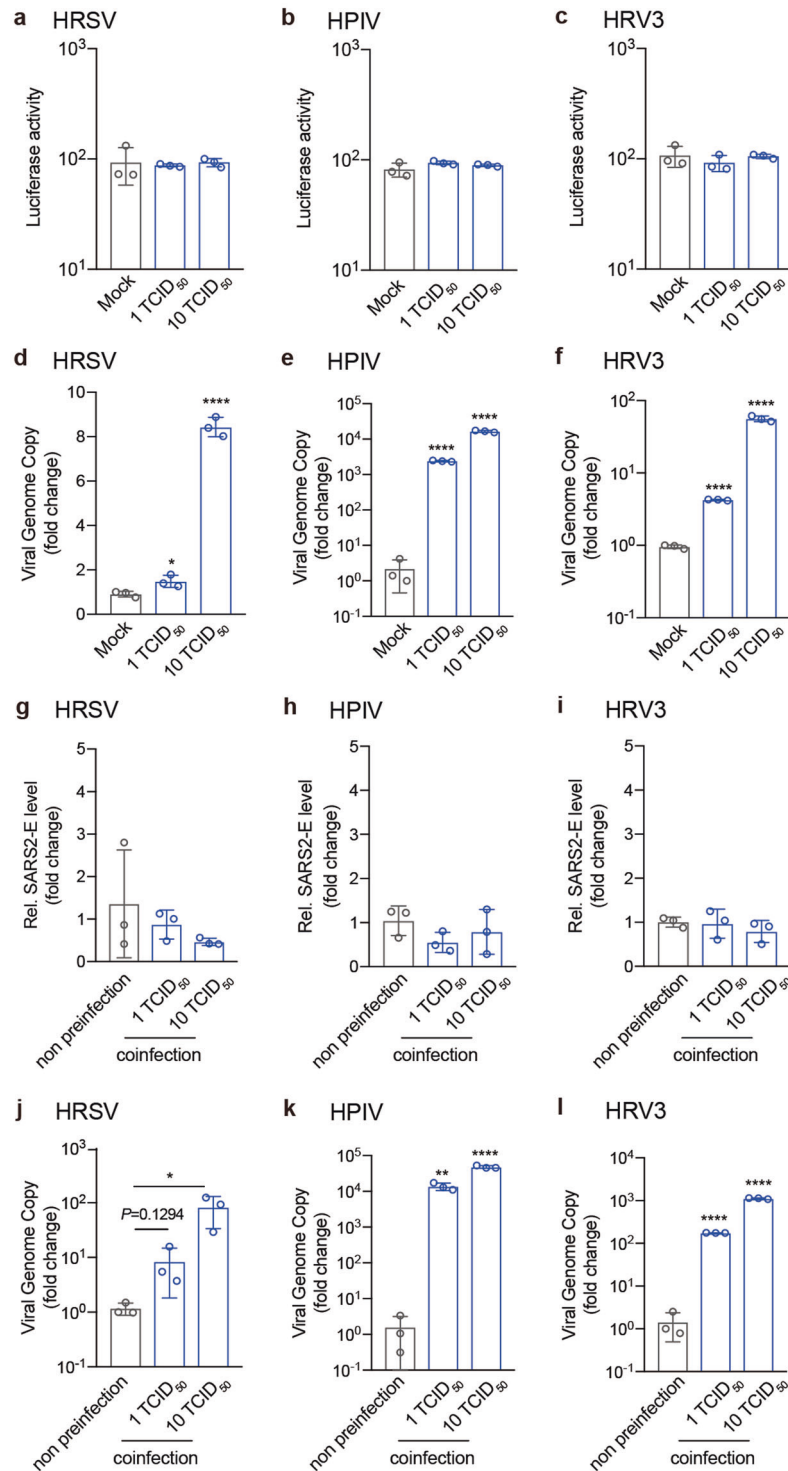
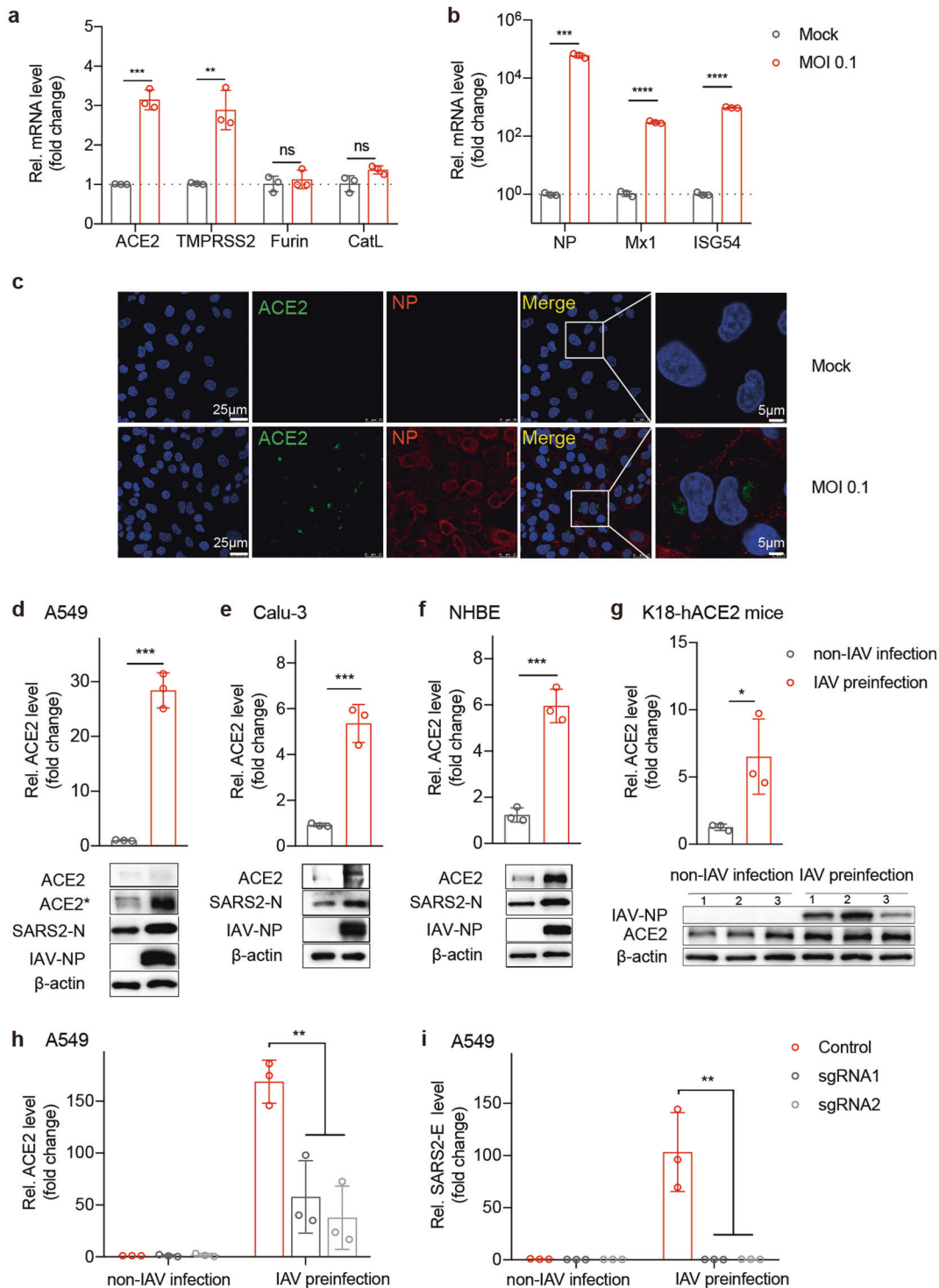


Fig. 3 SARS-CoV-2 infection in response to HRSV, HPIV, or HRV3. **a–c** A549 cells were preinfected with HRSV, HPIV, or HRV3 at the indicated doses for 12 h. Cells were then infected with pseudo-SARS-CoV-2 for another 24 h followed by measurement of luciferase activity. **d–f** The propagation of HRSV (**d**), HPIV (**e**), or HRV3 (**f**) in A549 cells was measured by qRT-PCR 12 h.p.i. targeting the individual viral genes respectively. **g–i** A549 cells were preinfected with HRSV (**g**), HPIV (**h**), or HRV3 (**i**) at the indicated doses for 12 h. Cells were then infected with live SARS-CoV-2 for another 48 h followed by measurement of SARS-CoV-2 E gene copies via Taqman-qRT-PCR. **j–l** The propagation of HRSV (**j**), HPIV (**k**), or HRV3 (**l**) in A549 cells was measured at 60 h.p.i. by qRT-PCR targeting the individual viral genes respectively. The data are expressed as fold changes relative to the non-preinfection group. Values represent means \pm SD of three independent experiments. * $P < 0.05$, ** $P < 0.01$, *** $P < 0.001$, **** $P < 0.0001$.



approximately threefold (A549 cells in Fig. 4a). An obvious switch in intracellular ACE2 expression was triggered at 12 h post-IAV infection (Fig. 4c). In addition, influenza NP, Mx1, and ISG54 increased accordingly, confirming successful IAV infection (Fig. 4b).

Interestingly, ACE2 mRNA levels increased more dramatically in IAV and SARS-CoV-2 coinfection cells, with 28-fold increase in A549 cells (Fig. 4d), fivefold increase in Calu-3 cells (Fig. 4e), and sixfold increase in NHBE cells (Fig. 4f). The mRNA and protein levels (Fig. 4g) of ACE2 also increased accordingly in lung

homogenates from coinfecting mice. We further detected the expression of ACE2, TMPRSS2, Furin, and Cat L under infection of HRSV, HPIV, or HRV3, respectively. The data show these viruses (unable to promote SARS-CoV-2 infection) had no effects on the expression of ACE2, TMPRSS2, Furin, and Cat L (Supplementary information, Fig. S3).

When cells were transfected by lentivirus encoding ACE2-sgRNA (small-guide RNA) to knockdown ACE2 expression (Fig. 4h), the IAV-mediated enhancement of SARS-CoV-2 infection was completely abolished (Fig. 4i).

Fig. 4 ACE2 is essential for IAV promotion of SARS-CoV-2 infection. **a, b** A549 cells were mock-infected or infected with WSN at an MOI of 0.1. At 12 h.p.i., total RNA was extracted from cells, and ACE2, TMPRSS2, Furin, and CatL mRNA levels (**a**) or NP, Mx1, and ISG54 mRNA levels (**b**) were evaluated via qRT-PCR using the SYBR green method. The data are expressed as fold changes relative to the mock infections. **c** A549 cells were infected with WSN at an MOI of 0.1. IAV NP protein (red) and ACE2 (green) were detected with an immunofluorescence assay at 12 h.p.i. Scale bars are shown. A549 (**d**), Calu-3 (**e**), and NHBE (**f**) cells were preinfected with WSN at an MOI of 0.1 for 12 h. Cells were then infected with live SARS-CoV-2 at an MOI of 0.01 for another 48 h. Total RNA was extracted from cells, and ACE2 mRNA was evaluated via qRT-PCR using the SYBR green method. The protein expression levels of ACE2, SARS-CoV-2 N gene, IAV NP, and β -actin were measured via western blotting assay. * means increased exposure to visualize ACE2. **(g)** The relative mRNA levels of ACE2 were measured in lung homogenates from the indicated groups, and the protein expression of IAV NP and ACE2 was detected via western blotting. **(d–g)** The data are expressed as fold changes relative to the non-IAV infection control. **(h–i)** To establish ACE2 knockdown cells, A549 cells were transduced with lentivirus encoding the CRISPR-Cas9 system with two guide RNAs targeting ACE2 (sgRNA1 and sgRNA2) or control guide RNA. Cells were infected with live SARS-CoV-2 at an MOI of 0.01 with or without IAV infection using the same procedure described above. The ACE2 (qRT-PCR) (**h**) and SARS-CoV-2 E gene (Taqman-qRT-PCR) (**i**) mRNA levels were detected. The data are expressed as the fold change relative to the non-IAV infection control. Values represent means \pm SD of three independent experiments. * $P < 0.05$, ** $P < 0.01$, *** $P < 0.001$, **** $P < 0.0001$.

These data indicate that IAV permitted increased SARS-CoV-2 infection mainly through upregulation of ACE2 expression.

Enhanced SARS-CoV-2 infectivity is independent of interferon signaling

ACE2 has been reported to be an interferon (IFN)-stimulated gene (ISG) in human airway epithelial cells.²⁰ IAV infection also stimulates type I IFN signaling. Therefore, we tested whether the augmentation of ACE2 expression is dependent on IFN. For this, cells were first pretreated with different doses of IFN α (Fig. 5) and IFN γ (Supplementary information, Fig. S4a–c) and then infected with pseudo-SARS-CoV-2. The data show that IFN α did not promote pseudo-SARS-CoV-2 infectivity in A549 cells (Fig. 5a) but rather significantly inhibited pseudo-SARS-CoV-2 infectivity in Calu-3 (Fig. 5d) and Huh-7 (Fig. 5g) cells. Compared with the mRNA levels of ISG54 (Fig. 5b, e, h), the mRNA levels of ACE2 and TMPRSS2 were only mildly increased by approximately 1- to 3-fold under IFN treatment (Fig. 5c, f, i). These data indicate that ACE2 could not robustly respond to IFN in these cells, which in turn suggest that ACE2-mediated viral entry was not affected by exogenous IFN.

Moreover, in IFNAR^{-/-} A549 cells, the enhanced infectivity of pseudo-SARS-CoV-2 under IAV coinfection was intact (Fig. 5j). In contrast to the decreased levels of ISG54 in IFNAR^{-/-} A549 cells (Fig. 5k; Supplementary information Fig. S4d), the mRNA levels of ACE2 and TMPRSS2 still increased in IFNAR^{-/-} A549 cells under IAV infection (Fig. 5l). Furthermore, in IFNAR^{-/-} A549 cells, the infectivity of live SARS-CoV-2 under IAV coinfection was again enhanced (Fig. 5m). These results strongly suggest that SARS-CoV-2 responded to IAV infection rather than endogenous IFN signaling for favorable viral infection.

DISCUSSION

Recently, there have been many discussions about the possible impacts of the upcoming flu season on the current COVID-19 pandemic. Speculations have been made that IAV infection could induce more severe disease due to secondary SARS-CoV-2 infection or that coinfection with these two viruses causes more serious illness. However, no experimental data are yet available to show the relationship between IAV and SARS-CoV-2. In this study, we provide the first experimental evidence that IAV preinfection strongly promotes SARS-CoV-2 virus entry and infectivity in cells and animals. These data emphasize that influenza prevention during the SARS-CoV-2 pandemic season is of great importance.

Coinfection of viruses frequently occurs in nature. Some studies have shown a positive interaction between dengue virus and Zika virus via antibody-dependent enhancement.²¹ Other studies have shown negative interactions between the common cold virus and SARS-CoV-2 via pre-existing immunity.²² Through coinfection with IAV and pseudotyped or live SARS-CoV-2, we observed a great enhancement in SARS-CoV-2 infectivity in both cell culture and

mice. This enhancement was associated with an increased expression level of ACE2, which is a major receptor for SARS-CoV-2 entry into host cells. We detected a 2- to 3-fold increase in ACE2 mRNA levels post-IAV infection (A549 cells). However, a much higher increase (28-fold) in the ACE2 mRNA level was detected after IAV and SARS-CoV-2 coinfection. We suspect that IAV infection induced mild expression of ACE2, permitting SARS-CoV-2 virus entry, and then, the subsequent multiplication of SARS-CoV-2 further enhanced ACE2 expression in a positive feedback pattern.²⁰ In K18-hACE2 mice, coinfection increased ACE2 expression by 6.5-fold under the airway epithelium-expressing human K18 promoter (less than that in A549 cells (28-fold) under the native hACE2 promoter). The lower induction fold of ACE2 in K18-hACE2 mice probably due to regulations at only post-transcriptional and translational levels because IAV and SARS-CoV-2 coinfection has no effects on hK18 promoter (data not shown). Nevertheless, Fig. 4i showed that the IAV-mediated enhancement of SARS-CoV-2 infection was completely abolished when ACE2 was knocked down, which again indicated that ACE2 is a major reason for SARS-CoV-2 enhancement although other factors may also play a role. The detailed mechanism still needs further studies.

Intriguingly, among the viruses tested, only IAV, but not HRSV, HPIV, HRV3, enhanced SARS-CoV-2 infection. The three viruses HRSV, HPIV, and HRV3 are prevalent pathogens that cause the common cold in humans, but these viruses had no effects on SARS-CoV-2 infectivity. Furthermore, we confirmed the universal effects of IAV through comparison of those of natural H1N1 and H3N2 isolates (Supplementary information, Fig. S5a), and also the influenza B virus (data not shown). In addition, the infectivity of the current D614G mutant SARS-CoV-2 can also be stimulated by IAV preinfection (Supplementary information, Fig. S5b). The unique ability of IAV to augment SARS-CoV-2 infectivity indicates that the influenza virus is a key pathogen requiring prevention and control during the current coronavirus pandemic.

As our data showed that IAV could still promote SARS-CoV-2 infection in IFNAR^{-/-} A549 cells (Fig. 5j, m), it suggests that endogenous IFN induced by IAV infection is not enough to inhibit SARS-CoV-2 infection. On the contrary, both our data with pseudo-SARS-CoV-2 (Fig. 5d, g) and others' data with either pseudo²³ or live SARS-CoV-2^{24,25} proved that exogenous IFN could strongly inhibit SARS-CoV-2 infection at least in cell cultures (probably through antiviral actions of numerous ISGs including IFMITS²³). Thus, we should distinguish the roles of endogenous and exogenous IFN in the coinfection model. Interestingly, the coinfection of IAV and SARS-CoV-2 mostly occurred in the same infected A549 cells (Supplementary information, Fig. S1b), further supporting that endogenous IFN plays limited roles in coinfection as it must act on the adjacent non-infected cells.

We further tested whether the expression of IAV gene segments alone could stimulate SARS-CoV-2 infection. The data in Supplementary information, Fig. S5c and S5d shows that segment-2

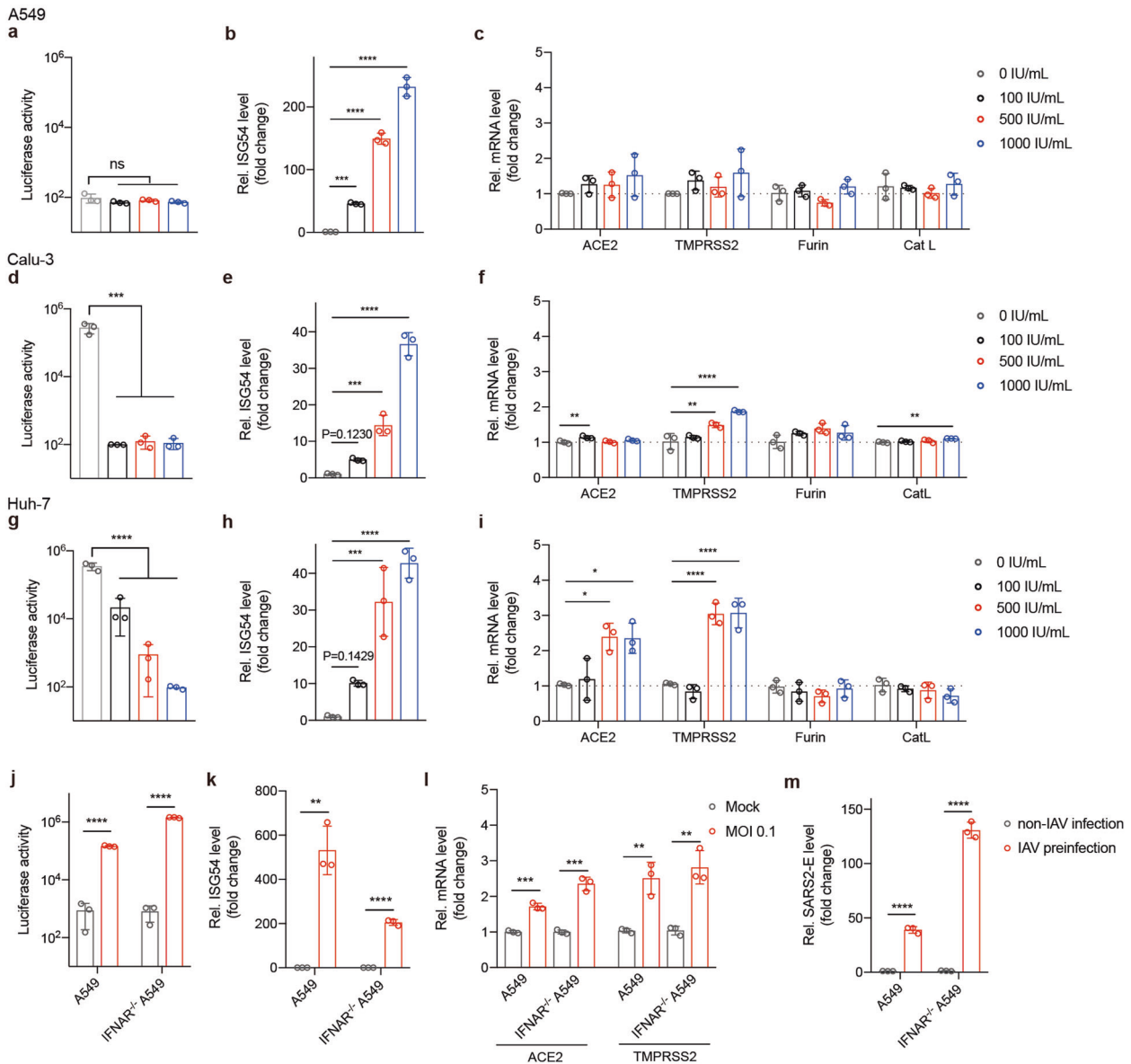


Fig. 5 Enhanced SARS-CoV-2 infection is independent of IFN signaling. A549 (a–c), Calu-3 (d–f), and Huh-7 (g–i) cells were pretreated with the indicated doses of IFN α for 12 h. Cells were then infected with pseudo-SARS-CoV-2 for another 24 h, followed by measurement of luciferase activity and the mRNA expression levels of the indicated genes. The mRNA levels are expressed as fold changes relative to nontreated cells. *P* values are from unpaired one-way ANOVA. j–l WT A549 and IFNAR $^{-/-}$ A549 cells were infected with WSN at an MOI of 0.1 for 12 h, and cells were then infected with pseudo-SARS-CoV-2 for another 24 h, followed by measurement of luciferase activity and the mRNA expression levels of the indicated genes. m WT A549 and IFNAR $^{-/-}$ A549 cells were infected with WSN at an MOI of 0.1 for 12 h, and the cells were then infected with live SARS-CoV-2 for another 48 h, followed by measurement of mRNA levels for SARS-CoV-2 E gene (Taqman-qRT-PCR). The data are expressed as fold changes relative to the nontreatment (b, c, e, f, h, i) or mock infection (k, l) or non-IAV infection (m) controls. Values represent means \pm SD of three independent experiments. **P* < 0.05, ***P* < 0.01, ****P* < 0.001, *****P* < 0.0001.

encoding PB1 showed the greatest promotive effect on SARS-CoV-2 infectivity and ACE2 expression. The detailed molecular mechanism underlying PB1-mediated SARS-CoV-2 enhancement needs further study. Nevertheless, the IAV segment-2 encodes two other viral proteins, PB1-F2, and PB1-N40, to modulate host cells.²⁶ PB1-F2 is a pro-apoptotic factor and can regulate innate immunity.²⁷ PB1-N40 interacts with many host factors and contributes to viral pathogenicity.²⁸ Overall, the fact that the IAV segment might promote SARS-CoV-2 infection further confirms a unique positive interaction between IAV and SARS-CoV-2.

Importantly, the enhancement phenotype in IAV and SARS-CoV-2 coinfection was independent of IFN signaling and was not observed when cells were coinfecting with inactivated IAV (data

not shown). Therefore, influenza vaccination (especially inactivated influenza vaccine) to inhibit influenza infection should be recommended to people with a high risk of coinfection. Our findings also remind that surveillance of coinfection is encouraged in the coming winter. Moreover, social distancing and mask-wearing are beneficial to protect people from the transmission of either or both viruses.

MATERIALS AND METHODS

Cells and viruses

The 293 T, A549, Huh-7, MDCK, Vero E6, WI-38, WI-38 VA-13, and BEAS-2B cells were obtained from ATCC and maintained in

Dulbecco's modified Eagle's medium (DMEM; Gibco) supplemented with 10% fetal bovine serum (FBS). The Calu-3 cells (ATCC) were maintained in DMEM supplemented with 20% FBS. NCI-H292 cells (ATCC) were maintained in RPMI-1640 (Gibco) supplemented with 20% FBS. Normal human bronchial epithelial cells (NHBE) cells (ATCC) were maintained in airway epithelial cell basal medium (ATCC PCS300030) supplemented with a Bronchial/Tracheal Epithelial Cell Growth Kit (ATCC PCS300040). All cells were incubated at 37 °C in 5% CO₂.

The A/WSN/33 virus was generated by reverse genetics as previously described.²⁹ H1N1 (A/Sichuan/01/2009) and H3N2 (A/Donghu/312/2006) were kindly provided by the Influenza Center in China CDC. HRV3 and HRSV were purchased from ATCC and stocked accordingly. HPIV was obtained from Professor Mingzhou Chen, Wuhan University. The SARS-CoV-2 live virus (strain IVCAS 6.7512) was provided by the National Virus Resource, Wuhan Institute of Virology, Chinese Academy of Sciences.

Plasmids and transfection

The plasmid encoding SARS-CoV-2-S-Δ18 was a gift from Professor Ningshao Xia, Xiamen University. The eight WSN viral segments in the pHW2000 plasmid were kindly provided by Professor Hans Klenk, Marburg University. The DNA transfection reagent Fugene HD was purchased from Promega, and the transfection was performed according to manuscript procedures.

Pseudotype virus production

Pseudotyped VSV-ΔG viruses expressing either a luciferase reporter or mCherry reporter were provided by Professor Ningshao Xia, Xiamen University. To produce pseudotyped VSV-ΔG-Luc/mCherry bearing SARS-CoV-2 spike protein (pseudo-SARS-CoV-2), Vero E6 cells were seeded in 10-cm dishes and transfected simultaneously with 15 μg SARS-CoV-2-S-Δ18 plasmid using Lipofectamine 3000 (Thermo). Forty-eight hours posttransfection, 150 μL pseudotyped VSV-ΔG bearing VSV-G protein was used to infect Vero E6 cells. Cell supernatants were collected after another 24 h, clearing of cell debris by centrifugation at 3000 rpm for 6 min, aliquoted, and stored at −80 °C.

Luciferase-based cell entry assay

Target cells were seeded in 48-well plates and inoculated in triplicate with equivalent volumes of pseudotyped virus stocks at a 1:5 dilution in DMEM (3% FBS) with or without IAV preinfection. At 24 h post-pseudotype infection, luciferase activities were measured with a Luciferase Assay System (Promega E4550).

Virus infection and IFN treatment

For IAV infection, cells were washed with PBS and then incubated with viruses at different MOIs (from 0.01 to 1) in infection medium (DMEM, supplemented with 2% FBS, 1% penicillin/streptomycin) at 37 °C in 5% CO₂.

For SARS-CoV-2 infection, cells were incubated with SARS-CoV-2 live virus at an MOI of 0.01 in infection medium (DMEM, 1% penicillin/streptomycin) and incubated at 37 °C in 5% CO₂ for 1 h with or without 12 h IAV preinfection (MOI 0.1). Cells were then washed with PBS two times and incubated in culture medium (DMEM, supplemented with 5% FBS and 1% penicillin/streptomycin) at 37 °C in 5% CO₂ for 48 h.

For HRV3, HPIV or HRSV infection, cells were washed with PBS and then incubated with the indicated viruses in infection medium (DMEM, supplemented with 3% FBS, 1% penicillin/streptomycin) and incubated at 37 °C in 5% CO₂ for 12 h.

For IFN treatment, recombinant human IFNα2a (Beyotime, P5646) and IFNγ (Beyotime, P5664) were dissolved in 0.1% BSA, diluted in DMEM with 10% FBS, and then incubated with cells for 12 h at the indicated doses.

Real-time reverse-transcriptase–polymerase chain reaction

The mRNA levels of the indicated genes were quantified via quantitative PCR with reverse transcription (qRT-PCR). Purified RNAs extracted with TRIzol (Invitrogen™, 15596018) were subjected to reverse transcription using oligo dT or random primer (using Takara cat#RR037A Kit), and then, the corresponding cDNAs were quantified using Hieff qPCR SYBR Green Master Mix (Yeason). Thermal cycling was performed in a 384-well reaction plate (ThermoFisher, 4343814). Quantification of IAV replication was measured by SYBR Green qRT-PCR with primers targeting NP vRNA, and the IAV expression was measured by SYBR Green qRT-PCR with primers targeting NP mRNA. Quantification of the propagation for other respiratory viruses was measured by SYBR Green qRT-PCR with primers targeting the HRSV M gene, the HPIV M gene, and the HRV3 5'UTR (position 456–569), respectively. Host receptor and cofactor genes were measured using gene-specific primers (Supplementary information, Table S1). All mRNA levels were normalized to the β-actin level in the same cell.

The relative number of SARS-CoV-2 viral genome copies was determined using a TaqMan RT-PCR Kit (Yeason). To accurately quantify the absolute number of SARS-CoV-2 genomes, a standard curve was prepared by measuring the SARS-CoV-2 N gene constructed in the pCMV-N plasmid. All SARS-CoV-2 genome copy numbers were normalized to GAPDH expression in the same cell.

All the primers and Tagman probes used in this study were listed in Supplementary information, Table S1.

Western blot analysis

For western blot analysis, cells were lysed in RIPA buffer on ice for 30 min, separated via sodium dodecyl sulfate-polyacrylamide gel electrophoresis (SDS-PAGE) and subjected to western blot analysis. For mouse experiments, half of the lung tissue from each mouse was homogenized in PBS, followed by boiling in SDS lysis buffer (GE) at 100 °C for 30 min. Rabbit monoclonal antibody against ACE2 (Abclonal, A4612, 1:1000), mouse monoclonal antibody against SARS-CoV Nucleoprotein (Sino Biological, 40143-MM05, 1:1000), and anti-actin antibody (Abclonal, 1:1000) were purchased commercially. The anti-influenza virus-NP antibody was kindly provided by Professor Ningshao Xia. Peroxidase-conjugated secondary antibodies (Antgene, 1:5000) were applied accordingly, followed by image development with a Chemiluminescent HRP Substrate Kit (Millipore Corporation).

Immunofluorescence

A549 cells were fixed and incubated with primary antibodies. The primary antibodies used in this study were rabbit polyclonal antibody against ACE2 for immunofluorescence (Sino Biological, 10108-T26) and anti-influenza virus-NP antibody (kindly provided by Professor Ningshao Xia). Alexa Fluor dye-conjugated secondary antibodies (Alexa Fluor R488, Invitrogen; Alexa Fluor M555, Invitrogen) and DAPI (Beyotime, C1002) were administered afterward according to standard protocols. Cell imaging was performed on a Leica TCS SP8 confocal laser scanning microscope (Leica).

ACE2 knockdown cells

Two sgRNAs targeting the hACE2 gene were designed under the protocol in <http://chopchop.cbu.uib.no> (sgRNA sequence of ACE2 were shown in Supplementary information, Table S1) and commercially synthesized to clone into the lenti-Cas9-blast vector (kindly provided by Professor Hongbing Shu). The control sgRNA lentivirus construct was also provided by Professor Hongbing Shu. In brief, A549 cells were plated in 6-well plates and transduced with lentivirus encoding the CRISPR-Cas9 system, including either ACE2 sgRNA or control sgRNA. The cell mixtures were selected with blasticidin for one week to obtain ACE2 knockdown cells. The gene knockdown efficiencies were confirmed by measuring the ACE2 mRNA level through qRT-PCR analysis.

Mice

K18-hACE2 transgenic mice, which express human ACE2 driven by the human epithelial cell cytokeratin-18 (K18) promoter used as an infection model for both SARS-CoV and SARS-CoV-2,^{30–32} were purchased from Gempharmatech and housed in ABSL-3 pathogen-free facilities under 12-h light-dark cycles with access to food and water. All animal experiments were approved by the Animal Care and Use Committee of Wuhan University. Mice were male, age-matched, and grouped for SARS-CoV-2 infection or IAV and SARS-CoV-2 coinfection. On day 0, mice were intranasally infected with PBS or 2000 PFU of WSN, and then, both groups were intranasally infected with 3×10^5 PFU of SARS-CoV-2 on day 2. Another two days later, mice were sacrificed to determine viral loads and for histological assays.

Histology analysis

Lung tissue from infected mice was dissected on day 2 post-SARS-CoV-2 infection, fixed, and stained using a standard Hematoxylin-Eosin staining (H&E) staining procedure. The slides were scanned and analyzed by the Wuhan Sci-Meds company. Representative images from three mice in each group are shown.

Statistical analysis

If not indicated otherwise, Student's *t*-test was used for two-group comparisons. **P* < 0.05, ***P* < 0.01, ****P* < 0.001, and *****P* < 0.0001 were considered significant. Unless otherwise noted, error bars indicate mean values and standard deviations of at least three biological experiments.

ACKNOWLEDGEMENTS

This work was supported in part by the National Key R&D Program (2018FYA0900801 to K.X. and 2016YFA0502103 to K.L.), the National Natural Science Foundation of China (grants 31922004 and 81772202 to K.X.), Application & Frontier Research Program of the Wuhan Government (2019020701011463 to K.X.), and Hubei Innovation Team Foundation (2020CFA015 to K.X. and K.L.).

AUTHOR CONTRIBUTIONS

K.X. and K.L. conceived the project and designed the experiments. L.B., J.D., M.G., X.W., Z.H., Z.Z., and Y.C. Z. coordinated the live SARS-CoV-2 study and performed animal infection experiments. Y.L. Z. and S. L. conducted pseudotyped virus infection experiments, IFN treatment experiments, and data analysis. L.B. and J.D. evaluated the immunofluorescence, histopathological and immunohistochemical studies. X.L. performed HRV3, HPIV, and HRSV infection experiments. Y.L. Z. and X. L. generated the mutant virus and performed the related tests. L.B., S.L., J.D., and X.L. repeated the key experiments in infected cells. X.S., Q.L., D.N., M.X., K.S., J.Y., W.Z., Z.T., M.T., Y.Z., C.S., M.D., L.Z., Y.C., and H.Y. provided technical support and materials. L. D. constructed ACE2 knockout cells and conducted related analysis. K.X., K.L., S.L., and Y.L. Z. wrote the manuscript with input from all the other authors. For their research spirit and courage, we also thank our group members of the SARS-CoV-2 working group in the State Key Laboratory of Virology, Wuhan University, who are working closely together during this new virus pandemic. We are grateful to Taikang Insurance Group Co., Ltd; Beijing Taikang Yicai Foundation; and Special Fund for COVID-19 Research of Wuhan University for their great supports of this work.

ADDITIONAL INFORMATION

Supplementary information accompanies this paper at <https://doi.org/10.1038/s41422-021-00473-1>.

Competing interests: The authors declare no competing interests.

REFERENCES

1. Huang, C. et al. Clinical features of patients infected with 2019 novel coronavirus in Wuhan, China. *Lancet* **395**, 497–506 (2020).

- Wang, C., Horby, P. W., Hayden, F. G. & Gao, G. F. A novel coronavirus outbreak of global health concern. *Lancet* **395**, 470–473 (2020).
- Van Riel, D. et al. Human and avian influenza viruses target different cells in the lower respiratory tract of humans and other mammals. *Am. J. Pathol.* **171**, 1215–1223 (2007).
- St. John, A. L. & Rathore, A. P. S. Early insights into immune responses during COVID-19. *J. Immunol.* **205**, 555 (2020).
- Traylor, Z. P., Aeffner, F. & Davis, I. C. Influenza A H1N1 induces declines in alveolar gas exchange in mice consistent with rapid post-infection progression from acute lung injury to ARDS. *Influenza and other respiratory. Viruses* **7**, 472–479 (2013).
- Hou, Y. et al. SARS-CoV-2 reverse genetics reveals a variable infection gradient in the respiratory tract. *Cell* **182**, 429–446 (2020).
- Belongia, E. & Osterholm, M. COVID-19 and flu, a perfect storm. *Science* **368**, 1163 (2020).
- Olsen, S. et al. Decreased influenza activity during the COVID-19 Pandemic - United States, Australia, Chile, and South Africa, 2020. *MMWR Morb. Mortal Wkly. Rep.* **69**, 1305–1309 (2020).
- Cuadrado-Payán, E. et al. SARS-CoV-2 and influenza virus co-infection. *Lancet* **395**, e84 (2020).
- Zheng, X. et al. Co-infection of SARS-CoV-2 and influenza virus in early stage of the COVID-19 epidemic in Wuhan, China. *J. Infect.* **81**, e128–e129 (2020).
- Yue, H. et al. The epidemiology and clinical characteristics of co-infection of SARS-CoV-2 and influenza viruses in patients during COVID-19 outbreak. *J. Med. Virology* **92**, 2870–2873 (2020).
- Xiong, H.L. et al. Robust neutralization assay based on SARS-CoV-2 S-protein-bearing vesicular stomatitis virus (VSV) pseudovirus and ACE2-overexpressing BHK21 cells. *Emerg. Microbes Infect.* **9**, 2105–2113 (2020).
- Zhou, P. et al. A pneumonia outbreak associated with a new coronavirus of probable bat origin. *Nature* **579**, 270–273 (2020).
- Wang, Q. et al. Structural and functional basis of SARS-CoV-2 entry by using human ACE2. *Cell* **181**, 894–904.e9 (2020).
- Lan, J. et al. Structure of the SARS-CoV-2 spike receptor-binding domain bound to the ACE2 receptor. *Nature* **581**, 215–220 (2020).
- Hoffmann, M. et al. SARS-CoV-2 cell entry depends on ACE2 and TMPRSS2 and is blocked by a clinically proven protease inhibitor. *Cell* **181**, 271–280.e278 (2020).
- Wu, C. et al. Furin, a potential therapeutic target for COVID-19. *iScience* **23**, 101642 (2020).
- Grimm, C. & Tang, R. Could an endo-lysosomal ion channel be the achilles heel of SARS-CoV-2? *Cell Calcium* **88**, 102212 (2020).
- Walls, A. C. et al. Structure, function, and antigenicity of the SARS-CoV-2 spike glycoprotein. *Cell* **181**, 281–292.e286 (2020).
- Ziegler, C. G. K. et al. SARS-CoV-2 receptor ACE2 is an interferon-stimulated gene in human airway epithelial cells and is detected in specific cell subsets across tissues. *Cell* **181**, 1016–1035.e1019 (2020).
- Priyamvada, L. et al. Human antibody responses after dengue virus infection are highly cross-reactive to Zika virus. *Proc. Natl. Acad. Sci. USA* **113**, 7852 (2016).
- Mateus, J. et al. Selective and cross-reactive SARS-CoV-2 T cell epitopes in unexposed humans. *Science* **370**, 89–94 (2020).
- Shi, G. et al. Opposing activities of IFITM proteins in SARS-CoV-2 infection. *EMBO J.* **0**, e106501 (2020).
- Vanderheiden, A. et al. Type I and Type III interferons restrict SARS-CoV-2 infection of human airway epithelial cultures. *J. Virol.* **94**, e00985–00920 (2020).
- Lokugamage, K. G. et al. Type I interferon susceptibility distinguishes SARS-CoV-2 from SARS-CoV. *J. Virol.* **94**, e01410–e01420 (2020).
- Wise, H. M. et al. A complicated message: Identification of a novel PB1-related protein translated from influenza A virus segment 2 mRNA. *J. Virol.* **83**, 8021–8031 (2009).
- Wang, R. et al. Influenza A virus protein PB1-F2 impairs innate immunity by inducing mitophagy. *Autophagy* <https://doi.org/10.1080/15548627.2020.1725375> (2020).
- Wise, H. et al. Overlapping signals for translational regulation and packaging of influenza A virus segment 2. *Nucleic Acids Res.* **39**, 7775–7790 (2011).
- Han, Q. et al. Sumoylation of influenza A virus nucleoprotein is essential for intracellular trafficking and virus growth. *J. Virology* **88**, 9379–9390 (2014).
- McCray, P. B. Jr et al. Lethal infection of K18-hACE2 mice infected with severe acute respiratory syndrome coronavirus. *J. Virology* **81**, 813–821 (2007).
- Zheng, J. et al. COVID-19 treatments and pathogenesis including anosmia in K18-hACE2 mice. *Nature* **589**, 603–607 (2021).
- Winkler, E. S. et al. SARS-CoV-2 infection of human ACE2-transgenic mice causes severe lung inflammation and impaired function. *Nat. Immunol.* **21**, 1327–1335 (2020).